JOURNAL OF APPLIED ELECTROCHEMISTRY 24 (1994) 1170–1175

Numerical simulation of two-dimensional fluid flow in electrochemical drilling

L. W. HOURNG, C. S. CHANG

Department of Mechanical Engineering, National Central University, Chung-Li, Taiwan 32054

Received 22 January 1993; revised 21 December 1993

A one-phase, two-dimensional fluid model is applied to predict the flow and thermal fields between electrodes in an electrochemical drilling (ECD) process. A body-fitted curvilinear coordinate transformation is used such that a moving, irregular surface of the workpiece in the physical domain becomes a fixed, regular boundary in the computational domain. The equilibrium workpiece shapes predicted by the present model agree in general with experimental results. Results show that some transport properties vary abruptly in the transition region. In the transition region, the rate of change of pressure in the streamwise direction is higher near the tool than near the workpiece. The electrolyte temperature near the surfaces of the workpiece and the tool in the transition and side regions is higher than that in other places.

1. Introduction

Electrochemical machining (ECM) is a process used to shape a piece of metal by high-rate electrochemical dissolution at its surface. The workpiece is the anode and the tool is the cathode. The electrolyte flows between the electrodes and carries away the dissolved metal. The main advantages of ECM [1] are: (i) the rate of metal machining does not depend on the hardness of the metal, (ii) complicated shapes can be machined on hard metals, and (iii) there is no tool wear. Recently, ECM has been widely applied in the aeronautics, space, and other high precision industries.

The metal removal rate is, in general, affected by the electric field and the flow field between the two electrodes. From the literature, research in predicting the workpiece shape can be classified into three categories. (i) By considering the effect of the electric field only: analytic techniques [2, 3] are basically limited to predicting the equilibrium workpiece shape with simple geometries. Various numerical techniques including the finite difference method (FDM) [4, 5], the finite element method (FEM) [6], and the boundary element method (BEM) [7] have also been applied. (ii) By considering the effect of the flow field only: either void fraction or temperature is taken into account in the majority of the papers [8–10]. Thorpe and Zerkle [11, 12] proposed a one-dimensional, two-phase, fluid flow model and showed that most ECM can be treated as a quasisteady process. (iii) By considering the effect of both electric and flow fields: Jain *et al.* [13] simulated ECM processes in which the metal removal rate is affected by the electric and flow fields. However, some electrolyte properties were assumed to vary along the flow path only and the governing equations of the flow field were much simplified. Hourng [14] solved a two-dimensional electric field and a one-dimensional, bubbly two-phase flow field to predict the workpiece shape and the variations of electrolyte properties between electrodes.

Thorpe and Zerkle [11, 12] mentioned that the influence of the flow field on the workpiece shape can not be neglected, especially near the transition region. Furthermore, the electrolyte flow may be two-dimensional in the transition region, where the gap between the electrodes changes rapidly. Therefore, a two-dimensional flow model is needed in predicting the workpiece shape machined by a tool of complex geometry, since the electrolyte flow may recirculate or separate around corners. A model, combing the equations of two-dimensional, one-phase flow and two-dimensional electric potential, is thus proposed in the present paper to simulate ECM. The prediction of the workpiece shape agrees well with experimental results. The variation of velocity, pressure and temperature of the electrolyte are demonstrated and analysed in detail. Understanding of the transport phenomena is helpful in the design of tool shape.

2. Theoretical model

2.1. *Electric field and variation of interelectrode gap*

Consider the electrochemical machining configuration sketched in Fig. 1. For convenience, an axially symmetric cavity is shown in which the electrolyte flow is radially outward. For quasisteady situations conservation of charge gives $\nabla' \cdot J' = 0$, where J' is the electric current density. From Ohm's law, $J' = -K'_e \nabla' \phi'$, where ϕ' is the electric potential and K'_e is the electrolyte electrical conductivity. In general, the electrolyte electrical conductivity may not be a constant due to temperature variation caused

0021-891X

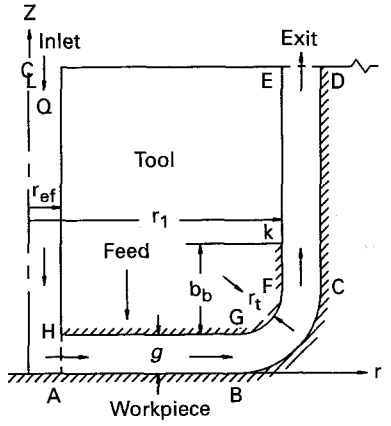

Fig. 1. A typical ECD configuration.

by Joule heating during the machining process. The distribution of the electric potential between the electrodes is thus governed by

$$\nabla' \cdot (K'_e \nabla' \phi') = 0 \tag{1}$$

The corresponding boundary conditions are

$$\left.\begin{aligned}
&\text{(i) } \phi' = \phi'_a, \quad \text{along } \overline{AB},\ \overline{BC} \text{ and } \overline{CD} \\
&\text{(ii) } \phi' = 0, \quad \text{along } \overline{HG},\ \overline{GF} \\
&\text{(iii) } \partial\phi'/\partial n = 0, \quad \text{along } \overline{AH},\ \overline{ED} \text{ and } \overline{EK} \\
&\text{(iv) } \phi' = 0 \text{ (bare bit tool),} \\
&\quad \text{or } \partial\phi'/\partial n = 0 \text{ (coated tool), along } \overline{FK}
\end{aligned}\right\} \tag{2}$$

where ϕ'_a is the applied voltage. The variation of the electrode gap g' is given by

$$\frac{\partial g'}{\partial t'} = V'_a - V'_c \tag{3}$$

where V'_c is the local tool feed velocity, and V'_a is the dissolution velocity of the anode in the direction normal to the tool surface. By Ohm's law and Faraday's law, Equation 3 can be written as

$$\frac{\partial g'}{\partial t'} = \frac{\epsilon \lambda_a j'}{\rho'_a} = f'_r \cos\theta \tag{4}$$

where λ_a is the electrochemical equivalent, ϵ the current efficiency, ρ'_a the anode density, and f'_r the feed rate of the cathode (tool). The current density normal to the workpiece, j', can be determined from the gradient of the electrical potential, ϕ', by

$$j' = K'_e \frac{\partial \phi'}{\partial n} \tag{5}$$

where n is the unit normal to the anode surface. The electrical conductivity of the electrolyte, K'_e, can be represented [11] by

$$K'_e = K'_0[1 + \gamma(T' - T'_0)] \tag{6}$$

where the zero subscript denotes the condition at the entrance of the electrode gap, γ the conductance constant, and T' the electrolyte temperature.

2.2. *Fluid equations*

In electrochemical drilling of a predrilled hole, the flow between electrodes contains the electrolyte, hydrogen gas and the dissolved metal. Since the amount of hydrogen gas and dissolved metal is small, the momentum and energy transport are determined by the electrolyte. The flow can thus be assumed to be incompressible, laminar and to contain only the electrolyte. The continuity and momentum equations of the axisymmetric flow can be expressed in cylindrical coordinates as

$$\frac{1}{r'}\frac{\partial}{\partial r'}(r'v'_r) + \frac{\partial}{\partial z'}(v'_z) = 0$$

$$v'_r\frac{\partial v'_r}{\partial r'} + v'_z\frac{\partial v'_r}{\partial z'} = -\frac{1}{\rho'}\frac{\partial P'}{\partial r'} + \frac{\mu'}{\rho'}\left[\frac{1}{r'}\frac{\partial}{\partial r'}\left(r'\frac{\partial v'_r}{\partial r}\right) + \frac{\partial^2 v'_r}{\partial z'^2} - \frac{v'_r}{r'^2}\right]$$

$$v'_r\frac{\partial v'_z}{\partial r'} + v'_z\frac{\partial v'_z}{\partial z'} = -\frac{1}{\rho'}\frac{\partial P'}{\partial z'} + \frac{\mu'}{\rho'}\left[\frac{1}{r'}\frac{\partial}{\partial r'}\left(r'\frac{\partial v'_z}{\partial r'}\right) + \frac{\partial^2 v'_z}{\partial z'^2}\right] \tag{7}$$

Dimensionless parameters are defined as follows:

$$r = r'/g'_e, \quad z = z'/g'_e, \quad v_r = v'_r/v'_0, \quad v_z = v'_z/v'_0, \quad P = \frac{P' - P'_e}{\rho' v'^2_0} \tag{8}$$

where the zero subscript denotes the condition at the entrance, g'_e the equilibrium gap at the entrance, and P'_e the exit pressure. Equation 7 can then be rewritten as

$$\frac{1}{r}\frac{\partial}{\partial r}(rv_r) + \frac{\partial}{\partial z}(v_z) = 0 \tag{9a}$$

$$v_r\frac{\partial v_r}{\partial r} + v_z\frac{\partial v_r}{\partial z} = -\frac{\partial P}{\partial r} + \frac{1}{Re}\left[\frac{1}{r}\frac{\partial}{\partial r}\left(r\frac{\partial v_r}{\partial r}\right) + \frac{\partial^2 v_r}{\partial z^2} - \frac{v_r}{r^2}\right] \tag{9b}$$

$$v_r\frac{\partial v_z}{\partial r} + v_z\frac{\partial v_z}{\partial z} = -\frac{\partial P}{\partial z} + \frac{1}{Re}\left[\frac{1}{r}\frac{\partial}{\partial r}\left(r\frac{\partial v_z}{\partial r}\right) + \frac{\partial^2 v_z}{\partial z^2}\right] \tag{9c}$$

where Re (the Reynolds number) $= \rho' v'_0 g'_e/\mu'$.

The incompressible Navier–Stokes Equations, namely Equations 9(a), (b) and (c), are non-linear and solved here by the vorticity-stream function approach [15]. The velocity components are firstly replaced by the vorticity, ζ, and the stream function, φ, defined as

$$\zeta = \frac{\partial v_r}{\partial z} - \frac{\partial v_z}{\partial r} \tag{10}$$

and

$$\frac{\partial \varphi}{\partial z} = rv_r, \qquad \frac{\partial \varphi}{\partial r} = -rv_z \tag{11}$$

respectively. By the elimination of the pressure term, Equations 9(b) and (c) can be combined and expressed in terms of the new dependent variables ζ and φ as

$$v_r\frac{\partial\zeta}{\partial r}+v_z\frac{\partial\zeta}{\partial z}-v_r\frac{\zeta}{r}=\frac{1}{Re}\left(\frac{\partial^2\zeta}{\partial r^2}+\frac{\partial^2\zeta}{\partial z^2}+\frac{1}{r}\frac{\partial\zeta}{\partial r}-\frac{\zeta}{r^2}\right) \tag{12}$$

Another equation involving the new dependent variables ζ and φ can be obtained by substituting Equation 11 into Equation 10. The final result is of the form

$$\frac{1}{r}\left(\frac{\partial^2\varphi}{\partial r^2}+\frac{\partial^2\varphi}{\partial z^2}-\frac{1}{r}\frac{\partial\varphi}{\partial r}\right)=\zeta \tag{13}$$

By differentiating Equation 9(b) with respect to r and Equation 9(c) with respect to z, respectively, and adding them, a partial differential equation governing the pressure distribution is obtained as

$$\frac{\partial^2P}{\partial r^2}+\frac{\partial^2P}{\partial z^2}+\frac{1}{r}\frac{\partial P}{\partial r}=2\left(\frac{\partial v_r}{\partial r}\frac{\partial v_z}{\partial z}-\frac{\partial v_z}{\partial r}\frac{\partial v_r}{\partial z}\right)-2\left(\frac{v_r}{r}\right)^2 \tag{14}$$

From Equations 12 and 13, ζ and φ can be determined by numerical iteration. The velocity components can be obtained from Equations 10 and 11. Since the velocity has been calculated, Equation 14 can thus be solved to get the pressure distribution.

The boundary conditions necessary in solving the flow field are described as follows. The exit pressure is given and the pressures along the other boundaries are calculated by the projection method [16]. Strictly speaking, the influence of the electrical potential distribution and the flow field variation in the inlet part on the workpiece shape can not be neglected, as mentioned by Novak [17]. However, the effect may become less as the diameter of the inlet decreases. For the sake of simplification, the section of $\overline{AH}$ is here taken as the inlet, where the velocity is given. Along the walls there is no slip and the velocity is fully-developed at the exit.

2.3. *Thermal field*

Since the electrolyte velocity and the corresponding Echert number are small, the energy dissipation can be neglected. By using the inlet temperature of the electrolyte as the characteristic temperature, the dimensionless form of the energy equation is

$$v_r\frac{\partial T}{\partial r}+v_z\frac{\partial T}{\partial z}=\frac{1}{PrRe}\left(\frac{\partial^2T}{\partial r^2}+\frac{\partial^2T}{\partial z^2}+\frac{1}{r}\frac{\partial T}{\partial r}\right)+W \tag{15}$$

where Pr (the Prandtl number) $=\mu' C_p'/k'$ and $W=W'g_e'/(\rho' C_p' T_0' v_0')$.

The energy generation rate, W', originating from the current, can be obtained by Joule's law as

$$W'=E'\cdot J'=K_e'\left[\left(\frac{\partial\phi'}{\partial r'}\right)^2+\left(\frac{\partial\phi'}{\partial z'}\right)^2\right] \tag{16}$$

where E' is the electrical intensity. The electrolyte properties, such as thermal conductivity k', constant pressure specific heat C_p', and viscosity coefficient μ' are assumed constant.

In solving the energy equation, the temperature at inlet, workpiece, and tool are specified, while the exit temperature is assumed fully developed.

2.4. *Numerical procedure*

In ECD, the workpiece shape is irregular and changes continuously during the machining process. To reduce the numerical errors caused by an improper mesh distribution near the boundaries of the physical domain, a body-fitted coordinate transformation technique is applied. In this technique, a Poisson equation is utilized to transform the irregular physical domain to the rectangular computational domain [18]. A smooth grid distribution is thus generated.

In this paper, electric potential, flow, and energy equations are all transformed to, and solved in, the computational domain. The spatial accuracy is of the order of $[(\Delta\xi)^2, (\Delta\eta)^2]$. All the numerical calculations are performed on an HP-9000/835 workstation, and a typical CPU time required for a case with grid size of 26×11 is about 284 s. The numerical procedure is as follows:

(i) Give the initial and boundary conditions.
(ii) Generate mesh distribution by the body-fitted coordinate transformation technique.
(iii) Calculate the distribution of electric potential.
(iv) Solve the flow field equations.
(v) Solve the energy equation.
(vi) Calculate the electrical conductivity and the metal dissolved rate.
(vii) Calculate the update workpiece shape.
(viii) Repeat steps (ii) to (vii) until the machining process reaches an equilibrium condition.

In steps (ii), (iii) and (v), the convergence criterion is that the relative error at each single node in the successive iterations is less than 10^{-3}. In step (iv), the pressure is said to be convergent when its relative error at every node in the successive iterations is less than 10^{-4}. Calculation terminates when the relative change of the workpiece shape in the successive time steps is less than 10^{-6} in the front region.

3. Results and discussion

In the present simulation of ECD, NaOH is used as the electrolyte. The properties of the electrolyte and the machining parameters are listed in Tables 1 and 2, respectively. For the sake of numerical stability [19], the initial gap between the electrodes is taken as twice that of the equilibrium gap. The volume flow rate and the viscosity of the electrolyte are assumed constant. The temperature of the workpiece and tool are constant and equal to that of the electrolyte at entrance. After numerous numerical tests, a grid size of 26×11 and a time-step of 30 s were found

Table 1. The physical properties of the electrolyte (NaOH solvent)

Temperature at entrance, T'_0/K	313.0
Specific heat ratio, C'_p/kJ kg^{-1} K^{-1}	4.18
Thermal constant, γ/K^{-1}	0.016
Density, ρ'/g cm^{-3}	1.06
Viscosity coefficient 10^{-3}, μ'/g cm^{-1} s^{-1}	7.81
Thermal conductivity, k'/W m^{-1} K^{-1}	0.63
Electrochemical equivalent 10^{-5}, λ_a/g C^{-1}	29.0

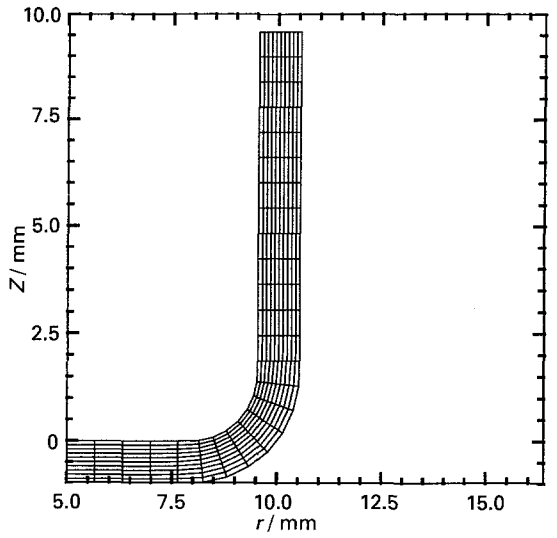

Fig. 2. The grid distribution in ECD.

to be reasonable in the consideration of the accuracy of the results and the consumption of CPU time. A typical grid distribution before machining is shown in Fig. 2. The meshes are smoothly distributed in general.

For ECD with a coated tool, comparisons between the experiments and the predictions in the equilibrium workpiece shape are shown in Fig. 3. Here SBFET [13] are the results predicted by the finite element method. Results show that the present prediction agrees well with the experiments, especially in the overcut region. The equilibrium gap between electrodes is maintained almost at the same value in the

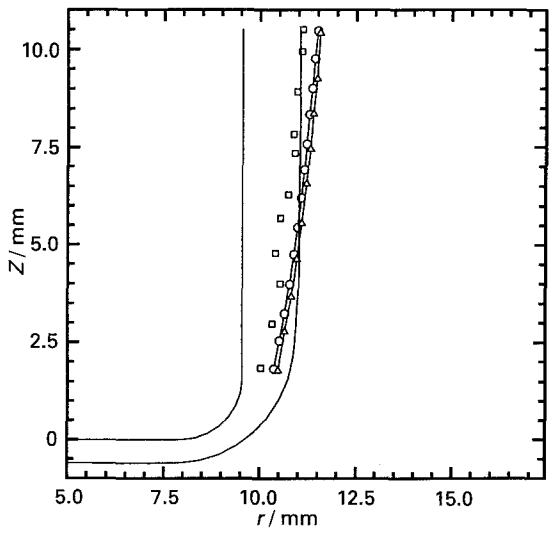

Fig. 3. Comparisons of the workpiece shape between numerical and experimental results. (□—□) Experimental [6]; (○—○) SBFET 11 [13]; (△–△) SBFET 22 [13]; (——) present.

Table 2. The machining parameters of ECD

Tool feed rate, f'_t/mm s^{-1}	0.00571
Averaged electric potential, ϕ'_a/V	14.89
Electrolyte electrical conductivity, K'_0/Ω^{-1} mm^{-1}	0.007
Tool radius, r_1/mm	9.54
Tool corner radius, r_t/mm	1.57
Electrolyte feed hole radius, r_{ef}/mm	5.0
Electrolyte velocity at entrance, v'_0/m s^{-1}	5.263
Current efficiency, ϵ/%	96.2

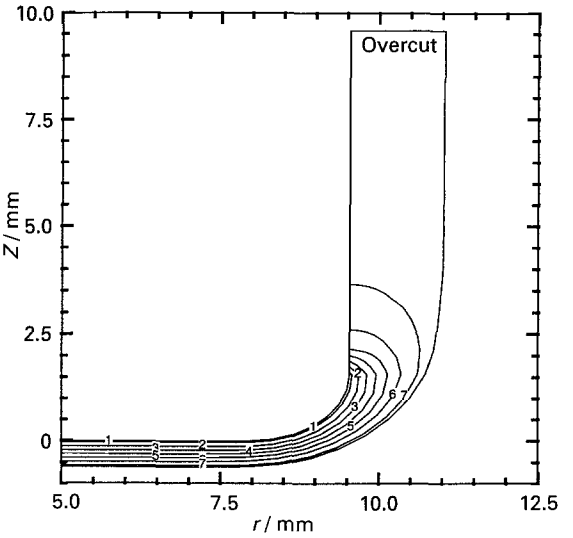

Fig. 4. Electric potential distribution in ECD with a side-coated tool. Key for FEE: (1) 0.92, (2) 3.09, (3) 5.26, (4) 7.44, (5) 9.61, (6) 11.79 and (7) 13.96 V.

front region ($r < 7.5$ mm). In the transition region, the gap remains almost constant before the corner, but it increases rather rapidly as the flow direction of the electrolyte changes. In the side region, the equilibrium gap is unchanged.

It is worth noting that the difference in the prediction of the workpiece overcut is about 2% as the influence of the flow and thermal fields is included or excluded. At first glance, it seems that the flow and thermal effects are insignificant in the prediction of ECD. However, the difference is expected to be

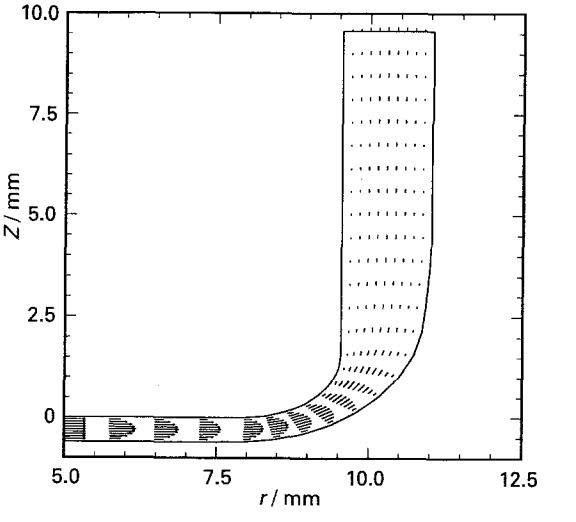

Fig. 5. Electrolyte velocity distribution in equilibrium. (——→) Unit vector: 5263 mm s^{-1}.

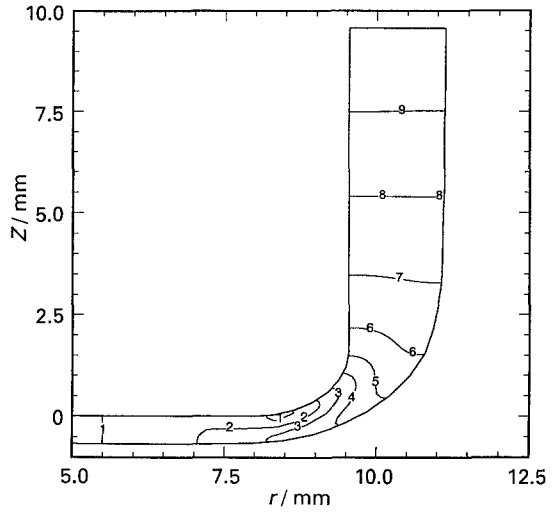

Fig. 6. Electrolyte pressure distribution in equilibrium. Pressure: (1) 0.895658, (2) 0.907252, (3) 0.918845, (4) 0.930439, (5) 0.942032, (6) 0.953626, (7) 0.965219, (8) 0.976812 and (9) 0.988406 atm.

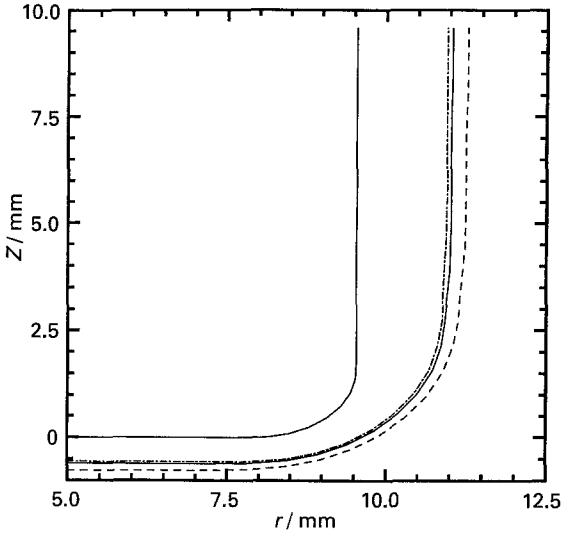

Fig. 8. The workpiece shapes in equilibrium for different tool feed rates. F_t: (– · – · –) 6.19×10^{-3}, (——) 5.71×10^{-3} and (– – – –) 4.50×10^{-3} mm s^{-1}.

large if the effect of the bubble void fraction on the electrolyte electrical conductivity is taken into account. Furthermore, the calculation of flow properties enables prediction of the electrolyte flow separation or recirculation, which can not be predicted if only the electric potential field is considered.

The variation of the electrolyte velocity in the gap is shown in Fig. 5. The tool and workpiece are geometrically axisymmetric and the electrolyte flow is radially outward in the front region from the centre of the tool. In the front region, the coss-sectional area through which the electrolyte flows is $\pi r^2 g$, where r is the radial distance from the centre of the inlet and g is the local gap width. As the electrolyte flow rate is kept constant, a large cross-sectional area implies a small electrolyte velocity from the viewpoint of conservation of mass. Therefore, the electrolyte velocity decreases gradually as it flows radially outward in the front region. The electrolyte velocity does not decrease further as the electrolyte flows from the front region into the transition region, where the gap between electrodes decreases. As the electrolyte moves downstream in the transition region, the interelectrode gap increases again. The electrolyte velocity is thus decelerated. In the side region, the electrolyte velocity is unchanged because the gap width is almost constant. The velocity profile of the electrolyte across the interelectrode gap is approximately parabolic with maximum velocity occurring along the centreline in the front and side regions. In the transition region, the electrolyte velocity near the workpiece is lower than that near the tool.

The electrolyte pressure distribution in the equilibrium condition is shown in Fig. 6. The pressure gradually increases downstream due to friction loss in both the front and side regions. In the transition region, the variation of the electrolyte pressure in the streamwise direction changes rapidly, especially near the tool corner where the curvature of the surface is large. However, in the gapwise direction, the electrolyte pressure near the workpiece is higher than that near the tool. This can be explained by the fact that the electrolyte velocity near the workpiece is

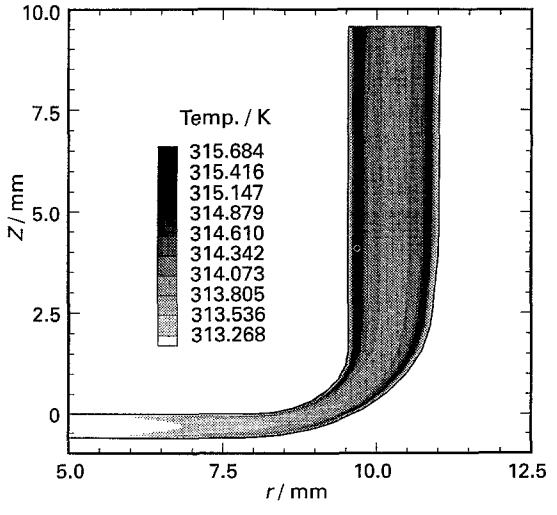

Fig. 7. Electrolyte temperature distribution in equilibrium.

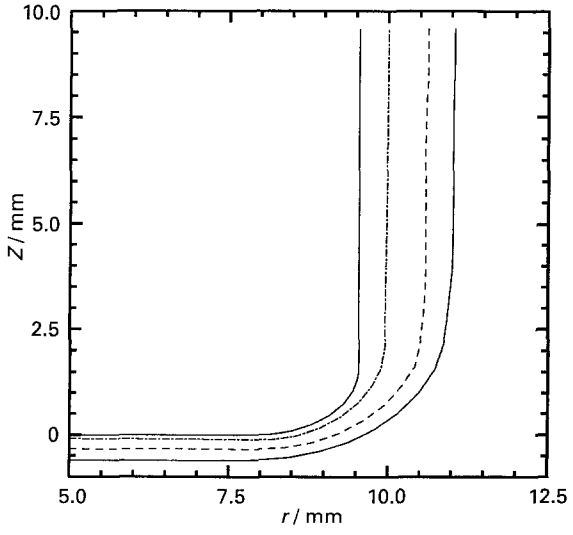

Fig. 9. The workpiece shapes in equilibrium for different applied voltages. FEE_a: (– · – · –) 3.00, (– – –) 8.00 and (——) 14.89 V.

lower than that near the tool, as mentioned previously. It is also worth noting that the highest rate of change of electrolyte pressure in the streamwise direction occurs near the tool in the transition region, where the possibility of separation of the electrolyte is higher than in other places.

Figure 7 shows the electrolyte temperature distribution in equilibrium. The heat generated by the throughput current is carried away by the electrolyte; therefore, the electrolyte temperature increases downstream. The rate of increase of the electrolyte temperature is slow in the front region, where the electrolyte velocity is high. However, heat is accumulated as the electrolyte velocity decreases in the transition and side regions. In the gapwise direction, the electrolyte temperature is higher near the workpiece and tool, where the electrolyte velocity is low and the effect of convective heat transfer is poor, than near the centreline region. However, the variation of the electrolyte temperature is too small to result in boiling of the electrolyte. The electrolyte's electrical conductivity is proportional to temperature, as can be seen from Equation 6. The distribution of the electrolyte electrical conductivity is thus similar to that shown in Fig. 7.

Figure 8 shows the workpiece shape for the tool with different feed rates. Results indicate that the workpiece shape is more congruent with the tool as the tool feed rate increases. As the tool feed rate increases from $5.71 \times 10^{-3}\,\mathrm{mm\,s^{-1}}$ to $6.19 \times 10^{-3}\,\mathrm{mm\,s^{-1}}$, the amount of decrease of the interelectrode gap in the front and side regions is about the same. Since the interelectrode gap in the front region is much less than that in the side region, the effect of the feed rate on the gap variation (in percentage) is larger in the front region than in the side region. To obtain a precise interelectrode gap in the front region, a high tool feed rate is therefore required.

The influence of the applied voltage on the workpiece shape is shown in Fig. 9. As the applied voltage increases, the overcut becomes large. Therefore, a low applied voltage is required for an accurate workpiece shape, though the machining time required is longer.

4. Conclusions

A theoretical model is used to simulate the transport properties in ECD. Results show that some transport properties, such as velocity, pressure, etc., vary abruptly in the transition region. In the transition region, the electrolyte pressure is higher near the workpiece than near the tool. However, the rate of change of pressure in the streamwise direction is lower near the workpiece than near the tool in the transition region. The electrolyte temperature near the workpiece and tool is higher than that in other places in both the transition and side regions. However, the variation of the electrolyte temperature is within 3 K for the present case. A high tool feed rate and a low applied electric voltage is desired to increase the accuracy of a ECD process.

In the present paper, the electrical conductivity of the electrolyte is assumed to be a function of temperature only but not void fraction. To improve the prediction, a two-phase, two-dimensional flow model must be used such that the influence of void fraction on the conductivity can be included.

References

[1] J. A. Mcgeough, 'Principles of Electrochemical Machining', John Wiley & Sons, New York (1974).
[2] D. E. Collett, R. C. Hewson-Brown and D. W. Windle, *J. Engineering Math.* **4** (1970) 29.
[3] P. Lawrence, Ph.D thesis, Leicester University, UK (1977).
[4] M. B. Nanayakkare, Ph.D thesis, University of Strathclyde, UK (1977).
[5] V. K. Jain and P. C. Pandey, *Precision Engineering* **2** (1980) 195.
[6] *Idem, Int. J. Math. Tool. Des. Res.* **22**(4), (1982) 341.
[7] O. H. Narayann, P. G. Yogindra and S. Murugan, *Int. J. Math. Tools Manufact.* **26**(3), (1980) 323.
[8] H. Tipton, Proceedings of the 5th international conference on machine tool research, Birmingham, UK, Sept. (1964) p. 509.
[9] K. Kawafune, T. Mikoshiba, K. Noto and K. Hirata, *CIRP Ann.* **15** (1967) 65/1–65/13.
[10] F. Hopenfeld and R. R. Cole, *J. Engng Industry, ASME Trans.* **88** (1966) 455.
[11] J. F. Thorpe and R. D. Zerkle, *Int. J. Mach. Tool Des. and Res.* **9** (1969) 131.
[12] *Idem*, 'Fundamentals of Electrochemical Machining', (edited by C. L. Faust), Princeton, NJ (1971) p. 1.
[13] V. K. Jain, P. G. Yogindra and S. Murugan, *Int. J. Mach. Tools Manufact.* **27**(1), (1987) 113.
[14] L. W. Hourng and C. S. Chang, *J. Appl. Electrochem.* **23** (1993) 316.
[15] D. A. Anderson, J. C. Tannehill and R. H. Pletcher, 'Computational Fluid Mechanics and Heat Transfer', McGraw-Hill Book Company, New York (1984).
[16] R. Peyret and T. D. Taylor, 'Computational Methods for Fluid Flow', Springer-Verlag, New York (1983).
[17] P. Novák, I. Roušar, A. Kimla, V. Mejta and V. Cezner, *Collection Czechoslovak Chem. Commun.* **46** (1981) 2949.
[18] J. P. Thompson, F. C. Thames and C. W. Mastin, *J. Comput. Phys.* **24** (1977) 274.
[19] L. W. Hourng and C. G. Chen, *J. Chinese Society Mech. Engng* **13**(2), (1992) 180.